

## Sublimation Growth of Bulk Aluminium Nitride Single Crystals With High Structural Perfection

M. Bickermann, C. Hartmann, J. Wollweber, A. Dittmar, C. Guguschev, F. Langhans

*Leibniz Institute for Crystal Growth (IKZ)  
Max-Born-Str. 2  
12489 Berlin, Germany  
Email: matthias.bickermann@ikz-berlin.de*

### INTRODUCTION

In recent years, single-crystalline aluminum nitride (AlN) became a candidate as substrate material for group-III nitride (Al,Ga,In)N epilayers [1]. AlN is fully miscible and chemically compatible to these compounds whilst being thermally and chemically most stable. The differences in lattice constants and thermal expansion (which causes additional strain during cooling down after epitaxy) are mitigated in heterostructures consisting of nitride layers with high Al content. Devices employing such heterostructures focus on the unique features found also in AlN, i.e., wide and direct band-gap of approx. 6.1 eV at room temperature [2], high thermal conductivity [3], and high electromechanical coupling (piezoelectricity) [4].

The use of AlN substrates with dislocation densities of  $10^3$ – $10^5$  cm<sup>-2</sup> leads to dislocation densities in the epilayers in the  $10^5$ – $10^6$  cm<sup>-2</sup> range [5, 6], mainly because the epitaxy technology of Al-rich nitrides is challenging and not well developed. However, Al-rich AlGaIn epitaxy on foreign substrates like sapphire or SiC yields dislocation densities of at least  $3 \cdot 10^8$  cm<sup>-2</sup> even when sophisticated growth techniques are employed [7]. Device efficiency (e.g. the charge carrier mobility, or the fraction of radiative recombination in optoelectronic emitters) has been shown to be very sensitive to structural quality and particularly to the dislocation density [8, 9]. It would thus greatly benefit from the use of AlN substrates. As a consequence, AlN substrates have been successfully employed for deep-UV optoelectronic emission [10], lasing [11], and sensor devices [12] as well as for mid-power GHz communication in high electron mobility transistors (HEMT) [13] and fast electroacoustic SAW and BAW devices [14].

AlN does not melt, but decomposes at approx. 2550°C at room pressure. The preferred method to grow AlN bulk single crystals is the sublimation–recondensation method also known as physical vapour transport (PVT). After an early breakthrough provided by Slack and McNelly in 1976/77 [15, 16] the huge progress made in PVT growth of silicon carbide in the 1990s has been very stimulating for AlN PVT growth. As AlN does not occur in nature and no seeds were initially available for bulk growth, three strategies for obtaining bulk crystals have been investigated: Grain selection, spontaneous nucleation, and growth on SiC as a foreign substrate [17]. The latter approach seemed especially promising to quickly reach AlN crystals of industrial relevant size and diameter [18], as SiC wafers with up to 4 inch in diameter are commercially available. However, the partial decomposition of SiC in the presence of gaseous Al leads to growth deterioration and contamination of the growing crystal with up to several atomic percent of silicon [19]. Furthermore, lattice and thermal expansion mismatch as well as defects present in the SiC seed or generated at the SiC/AlN interface lead to formation of grain boundaries and tilted domains [20, 21]. In particular, dislocation densities of the AlN crystals grown on SiC seeds typically exceed  $10^6$  cm<sup>-2</sup> [22] and do not decrease below  $10^5$  cm<sup>-2</sup> even after using such crystals as seeds for subsequent homoepitaxial growth.

In order to provide bulk AlN crystals with high structural perfection, we prepare AlN seeds by spontaneous nucleation and subsequent freestanding growth. This approach also mitigates the problem of stress-induced defect formation (or even cracking) which appears during grain selection where the crystal to be extended is surrounded by a parasitic polycrystalline rim [23]. Using proper growth conditions, freestanding AlN single crystals with c-plane areas exceeding 10 mm in diameter and a very high structural perfection can be prepared. We will further show that if homoepitaxial growth is performed on seeds prepared from such freestanding crystals, the high structural perfection is perpetuated even under growth conditions which allow for crystal enlargement.

### EXPERIMENTAL

All experiments are carried out in a RF-heated furnace (10 kHz, 30 kW) with a high purity nitrogen atmosphere (99.999%) at 60–900 mbar. Susceptor and insulation are made from high purity graphite and carbon bonded carbon fiber (CBCF), respectively. Temperatures are measured and controlled by infrared two-colour pyrometers on the lid and the bottom of the crucible. Commercially available AlN powder (HC Starck GmbH), pre-treated by sintering for 72 hours at 1900 °C, is used as AlN source material [24]. The residual AlN source contamination with oxygen is < 250 ppm. A crucible of sintered tantalum carbide [25] is employed for both native seed preparation by spontaneously nucleated freestanding AlN crystals and homoepitaxial seeding. In case of spontaneous nucleation and freestanding AlN growth, perforated tungsten plates act as nucleation centres in the centre of the crucible. The temperatures on the nucleation plate are varied between 2080°C and 2200°C. The growth times range from 60 h to 72 h. Homoepitaxial

seeding is carried out at seed temperatures of 2100 °C with 36 h to 48 h of growth time. Numerical calculations of thermal field (including conduction, radiation and convection heat exchange mechanisms) and mass transport (including diffusion and convective flow) are performed using the Virtual Reactor for AlN 6.2 code from STR Group Ltd.

The grown AlN crystals are sliced into 700 µm thick (0001) wafers by an inner diameter saw followed by mechanical polishing up to 1 µm using polycrystalline diamond. Optionally, the Al-polar surface is finished with a chemo-mechanical planarization process (CMP) or by Ar-ion etching with a Precision Etching Coating System (PECS) by GATAN. Defect etching is carried out at 350 °C for 3 minutes in a molten KOH/NaOH eutectic on the Al-polar surface. The rocking curves are recorded using a HRXRD diffractometer by GE Inspection & Sensing Technology. Optical transmission spectra are recorded at room temperature on a Perkin Elmer Lambda 19 UV/VIS Spectrometer. The impurity contents of oxygen and carbon of the grown crystals were measured on the {1010} facets by using secondary ion mass spectrometry (SIMS) performed by RTG, Berlin.

## RESULTS AND DISCUSSION

### Native seed preparation by spontaneous nucleation of freestanding AlN crystals

#### Thermodynamic considerations – determination of growth parameters

Sublimation and recondensation of AlN is represented schematically by the reaction  $\text{AlN(s)} \leftrightarrow \text{Al(g)} + \frac{1}{2} \text{N}_2\text{(g)}$ . Spontaneous nucleation and further growth of AlN single crystals with high structural perfection is only possible in a small parameter space with a moderate supersaturation of gaseous aluminium Al(g). A low supersaturation results in suppressed nucleation or very low growth rates, whereas a too high supersaturation leads to a high density of nucleation centres which eventually impedes enlargement and causes increased defect densities in the growing boule. At a given growth setup and a constant ambient pressure, the process parameters to be varied are the temperature at the growing surface  $T_{\text{growth}}$  and the temperature difference between the hottest point on the surface of the AlN source and the growth temperature ( $\Delta T = T_{\text{AlN-source-max}} - T_{\text{growth}}$ ). Both  $T_{\text{growth}}$  and  $\Delta T$  have a decisive influence on the supersaturation at the growing surface which is defined in Virtual Reactor for AlN 6.2 as

$$S = \frac{p_{\text{Al}}^2 * p_{\text{N}_2}}{K(T)} - 1 \quad (1)$$

The supersaturation  $S(T, \Delta T)$  was calculated in the interesting parameter space for the growth setup used (Fig. 1a). The supersaturation increases with increasing  $T_{\text{growth}}$  and  $\Delta T$  due to a strong increase in Al vapour pressure with temperature [26]. Three different growth regimes with moderate supersaturations ( $0,25 < S < 0,3$ ) were experimentally investigated. The conditions were

- (i)  $T_{\text{growth}} = 2080^\circ\text{C}$ ,  $\Delta T = 95\text{K}$ ,
- (ii)  $T_{\text{growth}} = 2150^\circ\text{C}$ ,  $\Delta T = 65\text{K}$ ,
- (iii)  $T_{\text{growth}} = 2200^\circ\text{C}$ ,  $\Delta T = 35\text{K}$ .

The calculated axial temperature profiles inside the crucible for the three growth regimes are shown in (Fig. 1b).

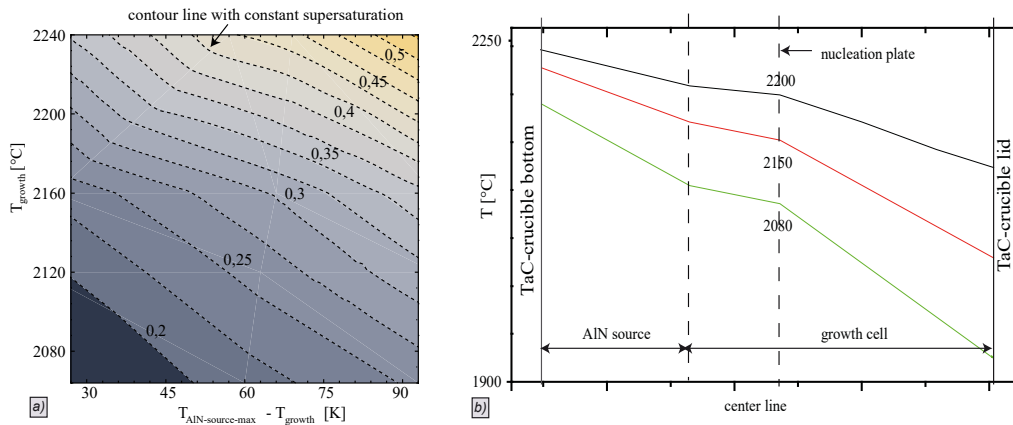


Fig. 1: a) contour plot of supersaturation  $S$  in dependence on  $T_{\text{growth}}$  and the temperature difference  $\Delta T = T_{\text{AlN-source-max}} - T_{\text{growth}}$  (calculated with Virtual Reactor for AlN 6.2); b) axial temperature profile with  $T_{\text{growth}}$  set to 2080, 2150, and 2200°C at the centre of the nucleation plate.

#### Habit and structural quality of freestanding AlN crystals

Growth rates in different crystallographic directions depend on their local growth temperature  $T_{\text{growth}}$  as well as on the temperature differences to neighbouring facets (i.e., the temperature distribution) and probably also orientation-dependent segregation effects of impurities [27]. This results in different crystal sizes and habits at different growth

temperatures. We found that the crystal habit changes completely with increasing growth temperature from c-oriented pillars (2080°C) to platelets with two opposing dominant m-plane faces (2150°C) and eventually to a nearly isometric habit (2200°C) as shown in Fig. 2. The growth rates are

- (i)  $R_{\parallel\langle 0001 \rangle} \approx 200 \mu\text{m/h}$  and  $R_{\perp\langle 0001 \rangle} \approx 50 \mu\text{m/h}$  for  $T_{\text{growth}} = 2080^\circ\text{C}$ ,
- (ii)  $R_{\parallel\langle 0001 \rangle} \approx 250 \mu\text{m/h}$  and  $R_{\perp\langle 0001 \rangle} \approx 30 - 250 \mu\text{m/h}$  for  $T_{\text{growth}} = 2150^\circ\text{C}$ ,
- (iii)  $R_{\parallel\langle 0001 \rangle} \approx R_{\perp\langle 0001 \rangle} \approx 250 \mu\text{m/h}$  for  $T_{\text{growth}} = 2200^\circ\text{C}$ .

In all growth conditions the habit is dominated by the stable N-polar  $\{000\bar{1}\}$  and prismatic  $\{10\bar{1}0\}$  facets. The  $\{0001\}$  facet is never observed. At locations where the AlN crystal expands at an angle in respect to the nucleation sheet,  $\{10\bar{1}n\}$  pyramidal facets are formed and cover the Al-polar bottom of the crystal. For  $T_{\text{growth}} = 2200^\circ\text{C}$ , the size of the  $\{10\bar{1}0\}$  and  $\{000\bar{1}\}$  planes easily reaches 9 mm and 14 mm, respectively.

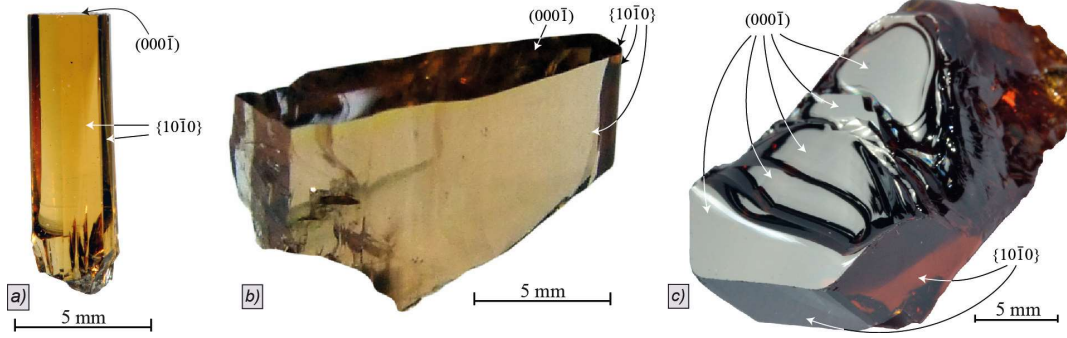


Fig. 2: Spontaneously nucleated freestanding AlN single crystals; a)  $\langle 0001 \rangle$  oriented pillar ( $T_{\text{Growth}} = 2080^\circ\text{C}$ ); b) platelets with two big  $\{10\bar{1}0\}$  faces ( $T_{\text{Growth}} = 2150^\circ\text{C}$ ); c) nearly isometric habit ( $T_{\text{Growth}} = 2200^\circ\text{C}$ ).

In all growth conditions, the crystals show a nearly perfect structural quality without small-angle grain boundaries and very low defect densities.  $\{0002\}$  and  $\{10\bar{1}0\}$  double crystal rocking curves (DCRC) are measured on  $\{000\bar{1}\}$  and  $\{10\bar{1}0\}$  as-grown facets, respectively. With open detector only one narrow peak with full width of half maximum (FWHM) values between 13 and 21 arcsec are recorded over the full as-grown facet areas (Fig. 3).

SIMS measurements on the as-grown m-plane  $\{10\bar{1}0\}$  facets show almost constant carbon concentrations for all growth regimes ( $[C] = 8 \pm 1 \times 10^{18} \text{cm}^{-3}$ ) and a decreasing oxygen concentration with increasing growth temperature ( $[O_{2080^\circ\text{C}}] = 4 \pm 1 \times 10^{19} \text{cm}^{-3}$ ,  $[O_{2150^\circ\text{C}}] = 3.2 \pm 0.6 \times 10^{19} \text{cm}^{-3}$  and  $[O_{2200^\circ\text{C}}] = 1.8 \pm 0.6 \times 10^{19} \text{cm}^{-3}$ ).

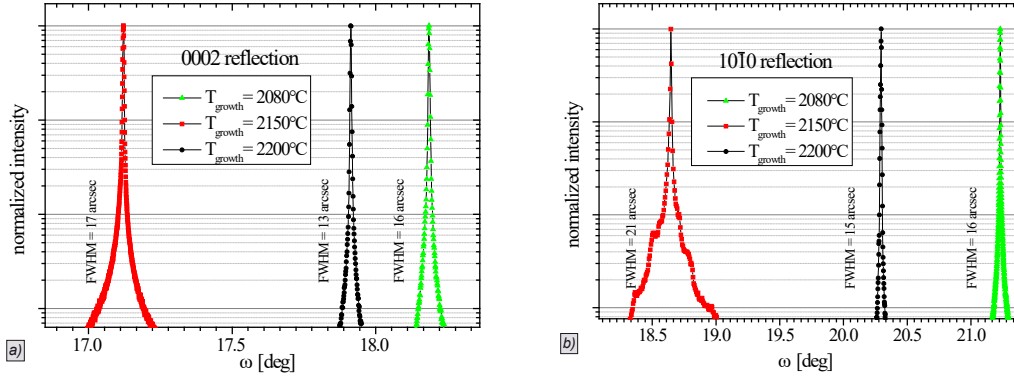


Fig. 3: Double crystal rocking curves (semi logarithmic scale) of freestanding AlN crystals measured with open detector over the full as-grown facet areas; a)  $\{0002\}$  reflection (measured over the  $\{000\bar{1}\}$  facet); b)  $\{10\bar{1}0\}$  reflection (measured over the  $\{10\bar{1}0\}$  facet). The absolute  $\omega$  values deviate from the theoretically values due to the tilt angles between the lattice planes of the AlN bulk crystals and the sample carrier plane in the measurement setup.

In contrast to seeded or epitaxial growth on a substrate, freestanding AlN crystals grow away from the nucleation plate from the hotter zone towards the colder zone of the crucible. Also, the growing surfaces do not face the AlN source directly. Thus, parasitic growth on the nucleation plate which consists of fine crystalline tungsten can be avoided. Also, as the nucleus forms directly on the plate, there is no void formation due to seed backside evaporation [21, 28]. Both the low impurity concentrations and the seedless growth without lattice mismatch or differences in thermal expansion promote the very high structural quality of the freestanding AlN crystals.

## Structural and optical properties of AlN wafers cut from isometric freestanding AlN crystals

Isometric crystals grown at 2200°C are sliced and polished into N-polar (000 $\bar{1}$ )-oriented wafers with about 8-10 mm in diameter which can be used as seeds in the homoepitaxial bulk growth process as well as substrates for device fabrication. The wafers typically show a zonar structure with a yellowish core area and a nearly colourless edge region (Fig. 4a). No structural defects such as small-angle grain boundaries or dislocation patterns are found at the boundary between these regions. The yellowish coloured area corresponds to the volume part which was grown on an N-polar (000 $\bar{1}$ ) facet; nearly colourless areas indicate that this volume part was grown on prismatic {10 $\bar{1}$ 0} facets. Thus, the yellowish area of a wafer reveals the size of the (000 $\bar{1}$ ) facet at the time when the wafer surface was the current growth interface during the freestanding AlN crystal growth process. Comparing the different wafers cut from one crystal, the yellowish area increases with the distance from the nucleation plate, which means that the N-polar (000 $\bar{1}$ ) facet expands as growth proceeds.

Fig. 4b shows the transmission and absorption spectra in the yellowish and nearly colorless regions of a double side polished {0001} wafer. Both curves show several absorption bands between 600 nm and the band edge at approx. 210 nm. The yellowish area reveals higher UV transparency as compared to the nearly colorless area. This is in accordance to earlier findings [27] in spite of the considerable differences in growth conditions (tungsten setup, Al polar seeded growth). The cause of the strong absorption below 300 nm has been identified as carbon on nitrogen site ( $C_N^-$ ) by Collazo et. al [29].

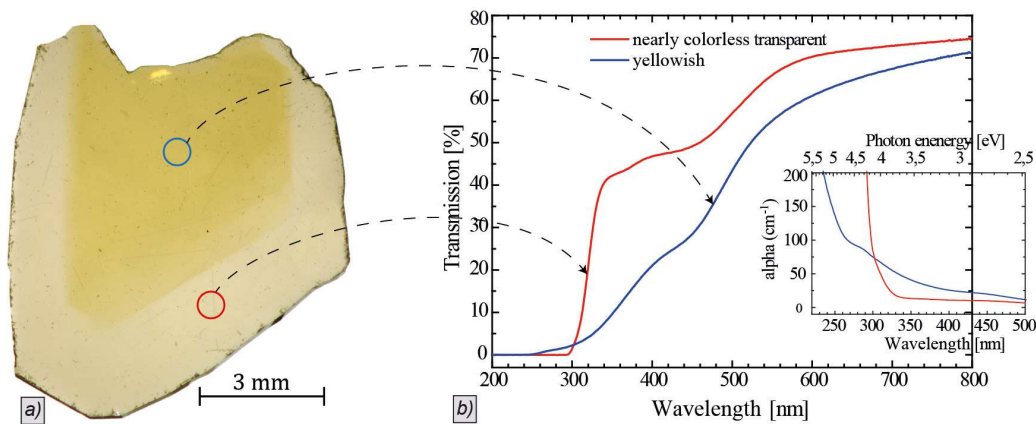


Fig. 4: a) Double side polished and Ar-ion etched {0001}-oriented wafer of 200  $\mu\text{m}$  thickness showing a zonar structure (yellowish core area and a nearly transparent edge region); b) transmission and absorption spectra of yellowish and transparent regions (recorded using aperture plates of 1 mm spot size).

Defect selective etching by KOH/NaOH eutectic on polished Al-polar (0001) AlN wafers shows a heterogeneous distribution of dislocations (Fig. 5). This observation is in line with investigations of Dalmau et. al. [30] on homoepitaxially grown bulk AlN crystals. The main areas of the wafers are virtually free of threading dislocations ( $\leq 100 \text{ cm}^{-3}$ ); some dislocation arrays are located in small clouds mostly in the {10 $\bar{1}$ 0} growth regions close to the wafer edges.

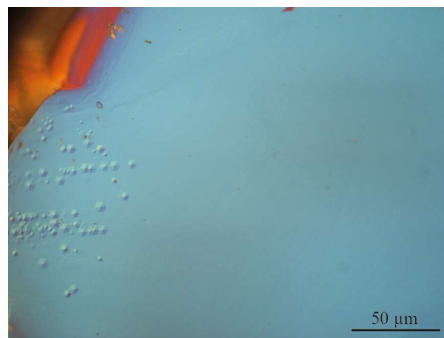


Fig. 5: Differential interference contrast (DIC) image of an Al-polar (0001) surface of an AlN wafer after etching in KOH/NaOH eutectic. Etch pits corresponding to threading dislocations (small dots) are found only close to the wafer edge (upper left corner).

X-ray Lang transmission topographs (Fig. 6b) are dominated by the residual surface defects from the mechanical polishing. Surface scratches and material fractures are distributed over the entire wafer surface. Nevertheless, the high structural quality of the wafer volume is verified. In accordance with the DCRC results, the full wafer is in diffraction

condition, i.e. small angle grain boundaries are absent. Large areas are dislocation free and only a few threading dislocation patterns close to the wafer edges exist, confirming the results of KOH/NaOH etching.

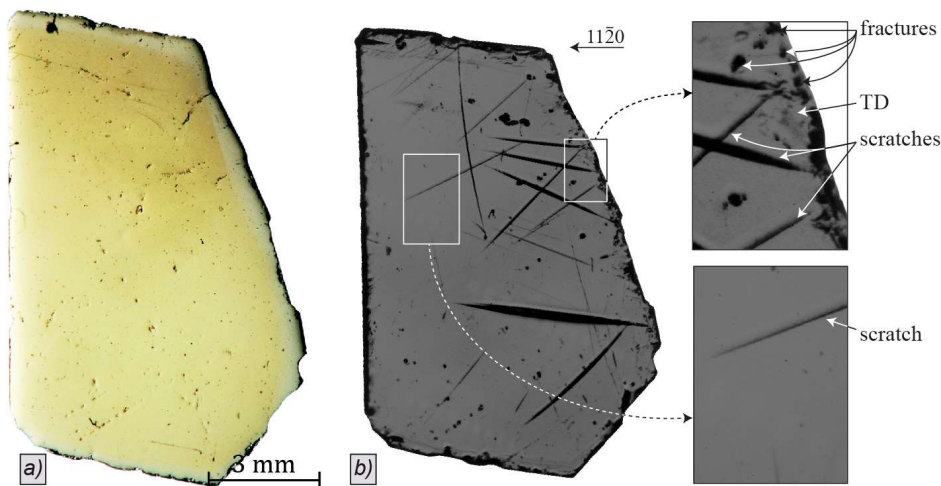


Fig. 6: Double side polished and Ar-ion etched  $\{0001\}$  wafer with zonal structure; a) optical transmission image; b) X-ray Lang transmission topograph with threading dislocations (TD) and residual surface defects from the mechanical polishing (surface scratches and material fractures).

### Homoepitaxial seeding on $(000\bar{1})$ wafers

$(000\bar{1})$ -oriented wafers with 8 mm in diameter cut from isometric freestanding crystals grown at  $2200^\circ\text{C}$  are polished and used as seeds in the homoepitaxial bulk growth process. A proprietary seed holder has been developed in order to ensure a smooth crystal enlargement preserving the high structural quality of the seeds without any parasitic growth around the growing single crystal. Fig. 7 shows a homoepitaxially grown crystal ( $T_{\text{seed}} = 2100^\circ\text{C}$ ,  $t = 48\text{ h}$ ) which enlarged from  $\text{Ø}8\text{ mm}$  to  $\text{Ø}12\text{ mm}$  over a growth distance of 10 mm. The average growth rate was approx.  $200\ \mu\text{m/h}$ . The facets dominating the crystal habit are again  $(000\bar{1})$  and  $\{10\bar{1}0\}$ . DCRC FWHM values on as-grown facets are 13–18 arcsec, thus structural quality is comparable to the spontaneously nucleated freestanding crystals.  $\{0001\}$  wafers cut from a homoepitaxially grown crystal are completely yellowish which indicates a uniform step flow growth mode on the  $(000\bar{1})$  facet [23]. Evaluation of dislocation density and impurity content is still ongoing.



Fig. 7: AlN single crystal; homoepitaxially grown on a  $(000\bar{1})$ -oriented wafer with 8 mm in diameter. The surface artefacts results from a touch of the growth interface with the source material at the end of the growth run.

### SUMMARY

PVT growth of freestanding AlN crystals is provided by using a tungsten sheet as nucleation plate placed in the middle of the crucible. At a nearly constant supersaturation of Al the crystal habit changes with increasing growth temperature ( $2080\text{--}2200^\circ\text{C}$ ) from  $\langle 0001 \rangle$  orientated pillars, to platelets, and to an isometric habit. In all growth conditions, the crystals show an almost perfect structural quality.

Wafers cut from freestanding crystals show a zonal structure with a yellowish core area and a nearly colourless edge region. Both, the defect selected etching and the X-ray topography of  $\{0001\}$  wafers reveal the higher defect density in the nearly transparent edge region which was grown on prismatic  $\{10\bar{1}0\}$  facets. The different incorporation of

impurities (mainly C and O) between the (000 $\bar{1}$ ) and {10 $\bar{1}$ 0} growth regions results in a lower deep-UV transparency in the edge regions.

First homoepitaxial AlN crystals were grown in step flow growth mode on (000 $\bar{1}$ ) seeds cut and polished from freestanding AlN crystals grown at 2200°C. A smooth crystal enlargement preserving the high structural quality of the seeds without any parasitic growth around the growing single crystal could be provided.

The AlN single crystals with very low dislocation densities and without small-angle grain boundaries might be used as substrates for improved UV optoelectronic and high power devices.

## REFERENCES

- [1] D. Ehrentraut, Z. Sitar, MRS Bulletin, 34 (2009) 259-265.
- [2] M. Feneberg, R.A.R. Leute, B. Neuschl, K. Thonke, M. Bickermann, Physical Review B, 82 (2010) 075208.
- [3] G.A. Slack, R.A. Tanzilli, R.O. Pohl, J.W. Vandersande, Journal of Physics and Chemistry of Solids, 48 (1987) 641-647.
- [4] C. Deger, E. Born, H. Angerer, O. Ambacher, M. Stutzmann, J. Hornsteiner, E. Riha, G. Fischerauer, Applied Physics Letters, 72 (1998) 2400-2402.
- [5] R.T. Bondokov, S.G. Mueller, K.E. Morgan, G.A. Slack, S. Schujman, M.C. Wood, J.A. Smart, L.J. Schowalter, Journal of Crystal Growth, 310 (2008) 4020-4026.
- [6] R. Dalmau, B. Moody, R. Schlessler, S. Mita, J. Xie, M. Feneberg, B. Neuschl, K. Thonke, R. Collazo, A. Rice, J. Tweedie, Z. Sitar, J. Electrochem. Soc. , 158 (2011) H530.
- [7] H. Hirayama, S. Fujikawa, J. Norimatsu, T. Takano, K. Tsubaki, N. Kamata, physica status solidi (c), 6 (2009) S356-S359.
- [8] Y. Taniyasu, M. Kasu, Diamond and Related Materials, 17 (2008) 1273-1277.
- [9] M. Kneissl, T. Kolbe, C. Chua, V. Kueller, N. Lobo, J. Stellmach, A. Knauer, H. Rodriguez, S. Einfeldt, Z. Yang, N.M. Johnson, M. Weyers, Semiconductor Science and Technology, 26 (2011) 014036.
- [10] J.R. Grandusky, S.R. Gibb, M.C. Mendrick, C. Moe, M. Wraback, L.J. Schowalter, Applied Physics Express, 4 (2011).
- [11] T. Wunderer, C.L. Chua, Z.H. Yang, J.E. Northrup, N.M. Johnson, G.A. Garrett, H.G. Shen, M. Wraback, Applied Physics Express, 4 (2011).
- [12] T. Erlbacher, M. Bickermann, B. Kallinger, E. Meissner, A.J. Bauer, L. Frey, physica status solidi (c), 9 (2012) 968-971.
- [13] X. Hu, J. Deng, N. Pala, R. Gaska, M.S. Shur, C.Q. Chen, J. Yang, G. Simin, M.A. Khan, J.C. Rojo, L.J. Schowalter, Applied Physics Letters, 82 (2003) 1299-1301.
- [14] G. Bu, D. Ciplys, M. Shur, L.J. Schowalter, S. Schujman, R. Gaska, IEEE Trans. Ultrason. Ferroelectr. Freq. Control, 53 (2006) 251-254.
- [15] G.A. Slack, T.F. McNelly, Journal of Crystal Growth, 34 (1976) 263-279.
- [16] G.A. Slack, T.F. McNelly, Journal of Crystal Growth, 42 (1977) 560-563.
- [17] B.M. Epelbaum, M. Bickermann, A. Winnacker, Journal of Crystal Growth, 275 (2005) 479-484.
- [18] Y.N. Makarov, O.V. Avdeev, I.S. Barash, D.S. Bazarevskiy, T.Y. Chemekova, E.N. Mokhov, S.S. Nagalyuk, A.D. Roenkov, A.S. Segal, Y.A. Vodakov, M.G. Ramm, S. Davis, G. Huminic, H. Helava, Journal of Crystal Growth, 310 (2008) 881-886.
- [19] M. Bickermann, O. Filip, B.M. Epelbaum, P. Heimann, M. Feneberg, B. Neuschl, K. Thonke, E. Wedler, A. Winnacker, Journal of Crystal Growth, 339 (2012) 13-21.
- [20] M. Bickermann, B.M. Epelbaum, O. Filip, P. Heimann, S. Nagata, A. Winnacker, phys. stat. sol. (c), 5 (2008) 1502-1504.
- [21] C. Hartmann, M. Albrecht, J. Wollweber, J. Schuppang, U. Juda, C. Guguschev, S. Golka, A. Dittmar, R. Fornari, Journal of Crystal Growth, 344 (2012) 19-26.
- [22] P. Lu, J.H. Edgar, C. Cao, K. Hohn, R. Dalmau, R. Schlessler, Z. Sitar, Journal of Crystal Growth, 310 (2008) 2464-2470.
- [23] Z.G. Herro, D. Zhuang, R. Schlessler, Z.Sitar, Journal of Crystal Growth, 312 (2010) 2519-2521.
- [24] C. Hartmann, J. Wollweber, C. Seitz, M. Albrecht, R. Fornari, Journal of Crystal Growth, 310 (2008) 930-934.
- [25] A. Dittmar, C. Guguschev, C. Hartmann, S. Golka, A. Kwasniewski, J. Wollweber, R. Fornari, Journal of the European Ceramic Society, 31 (2011) 2733-2739.
- [26] B.M. Epelbaum, M. Bickermann, A. Winnacker, Materials Science Forum, 457-460 (2004) 1537-1540.
- [27] M. Bickermann, B.M. Epelbaum, O. Filip, B. Tautz, P. Heimann, A. Winnacker, physica status solidi (c), 9 (2012) 449-452.
- [28] O. Filip, B.M. Epelbaum, M. Bickermann, P. Heimann, A. Winnacker, Journal of Crystal Growth, 318 (2011) 427-431.
- [29] R. Collazo, J.Q. Xie, B.E. Gaddy, Z. Bryan, R. Kirste, M. Hoffmann, R. Dalmau, B. Moody, Y. Kumagai, T. Nagashima, Y. Kubota, T. Kinoshita, A. Koukitu, D.L. Irving, Z. Sitar, Applied Physics Letters, 100 (2012) 191914.
- [30] R. Dalmau, B. Moody, J. Xie, R. Collazo, Z. Sitar, physica status solidi (a), 208 (2011) 1545-1547.